Table 1. Basic electrophysiological properties of Purkinje cells

	Membrane capacitance (pF)[a,d]	Resting membrane potential (mV)[a]	Input resistance (MΩ)[a,d]	Percentage of cells showing spontaneous action potentials[b,e]	Frequency of spontaneous action potentials (Hz)[c,e]
GFP alone	39.2 ± 24.3 ($n = 35$)	−58.3 ± 13.6 ($n = 35$)	379 ± 278 ($n = 35$)	80% (12 of 15 cells)	0.43 ± 1.00 ($n = 15$)
WT mKv3.3	40.1 ± 16.1 ($n = 17$)	−59.9 ± 8.24 ($n = 17$)	367 ± 181 ($n = 17$)	75% (6 of 8 cells)	0.25 ± 0.59 ($n = 8$)
R424H mutant	22.3 ± 6.9*† ($n = 28$)	−59.5 ± 7.4 ($n = 28$)	372 ± 169 ($n = 28$)	64% (9 of 14 cells)	0.12 ± 0.75 ($n = 14$)

Here and in Table 2, statistical analysis was conducted between cells expressing the R424H mutant and those expressing green fluorescent protein (GFP) alone or between cells expressing R424H mutant and those expressing wild-type (WT) mKv3.3. Data are given as the means ± SD, and n is the number of experiments. *$P < 0.001$ between GFP alone and R424H mutant. †$P < 0.001$ between WT mKv3.3 and R424H mutant. The statistical analysis indicated by superscript letters a, b and c was conducted using Student's unpaired t test, the χ^2 test and Mann–Whitney U test, respectively. [d]Membrane capacitance and input resistance were measured in voltage-clamp conditions. [e]Spontaneous action potentials were recorded at resting membrane potential for 300 s.

compared with PCs expressing GFP alone or those expressing WT subunits (Table 1; resting membrane potential, R424H *versus* GFP, $P = 0.533$; R424H *versus* WT, $P = 0.874$; and input resistance, R424H *versus* GFP, $P = 0.882$; R424H *versus* WT, $P = 0.913$; analyses by Student's unpaired t test). Spontaneous action potentials were also observed in some PCs in all groups (Table 1 and Supplemental Fig. S4*B* and *C*). The percentages of PCs generating spontaneous firing and the frequency of the firing were comparable among the three groups (Table 1).

Outward currents were recorded in Hepes-buffered ACSF containing TTX, $CdCl_2$, picrotoxin and DNQX (see Methods). Representative current traces recorded from GFP-, WT- and R424H mutant-expressing PCs are illustrated in Fig. 4*A*. Depolarizing voltage pulses (more positive than −10 mV) evoked outward currents with a transient peak in GFP-, WT- and R424H mutant-expressing PCs (Fig. 4*A*). In WT-expressing PCs, peak amplitudes of the transient currents were larger than those in GFP-expressing PCs, indicating that lentivirally expressed mKv3.3 formed functional channels (Fig. 4*Ab*). In contrast, the peak amplitudes in R424H mutant-expressing PCs were smaller than those in GFP-expressing PCs (Fig. 4*Aa* and *Ac*). As the membrane capacitance of R424H mutant-expressing PCs was significantly smaller than that of GFP- and WT-expressing PCs (Table 1), the peak current amplitudes at voltages between +10 and +40 mV were normalized to membrane capacitances (current densities, in pico-amperes per picofarad; Fig. 4*B*). The current densities in R424H mutant-expressing PCs were ∼2-fold smaller than those in GFP-expressing PCs at voltages between +10 and +40 mV (Fig. 4*B*), confirming that the expression of the R424H mutant subunits in cultured PCs suppressed outward currents in a dominant-negative manner.

Expression of R424H mutant subunits reduces sEPSCs in PCs

In standard culture conditions, PCs receive excitatory synaptic inputs from granule cells via the dendrites (Hirano *et al.* 1986; Hirano & Kasono, 1993). In order to examine how R424H mutant-induced impairment of dendritic development affects the synaptic inputs to PCs, sEPSCs were recorded from PCs in the presence of picrotoxin at a holding potential of −80 mV (Fig. 5). Examples of sEPSCs in GFP- or WT-expressing PCs appear as downward deflections in the current traces (Fig. 5*Aa* and *Ba*). These currents were abolished by application of 20 μM DNQX (traces not shown) and were thus identified as being mediated by AMPA/kainate receptors. Ensemble averages of the events in individual cells are also shown in Fig. 5*Ab* and *Bb*. Although sEPSCs in both groups were observed in all cells tested (Table 2), most R424H mutant-expressing PCs (10 of 13 cells) did not show sEPSCs during the 250 s recording period (Fig. 5*C* and Table 2; R424H and GFP, $P < 0.001$; R424H and WT, $P < 0.001$ by Fisher's exact probability test). Even in PCs showing sEPSCs, the frequency was significantly lower than in GFP- or WT-expressing PCs (Table 2). The R424H mutant-expressing PCs might receive few, if any, excitatory synaptic contacts onto their somata and dendrites.

R424H mutant-expressing PCs exhibit broadened action potentials and altered firing patterns

Expression of R424H mutant subunits in PCs suppressed outward current density, suggesting the alteration of the action potential waveform and firing properties in R424H mutant-expressing PCs. To examine these possibilities,

single action potentials (Fig. 6) and repetitive firings (Fig. 7) were evoked in current-clamp conditions. When a single action potential was evoked by short current injection (10 ms duration), R424H mutant-expressing PCs showed a broadened action potential waveform (Fig. 6*A*). The half-amplitude widths of R424H mutant-expressing PCs were 1.7-fold larger than those of GFP-expressing PCs (Fig. 6*B*; $P < 0.001$). The maximal rate of rise and maximal rate of fall in R424H mutant-expressing PCs were 0.75- and 0.65-fold of those in GFP-expressing PCs, respectively (Fig. 6*C* and *D*; maximal rate of rise, $P < 0.001$; maximal rate of fall, $P < 0.001$). These changes suggest that not only outward K^+ current but also voltage-dependent Na^+ current (I_{Na}) was affected by the expression of R424H mutant, because the maximal rate of rise of the action potential has been used as an index of the inward I_{Na} (Hodgkin & Katz, 1949).

To clarify the reduction of the maximal rate of rise by R424H mutant expression, I_{Na} was recorded from PCs in voltage-clamp conditions (Supplemental Fig. S5). Expression of R424H mutant subunits significantly reduced I_{Na} compared with the control group, without any changes in the voltage dependence of activation and inactivation. As the I_{Na} of cultured PCs is distributed through the cell body and axons (Fry *et al.* 2007), the reduction in I_{Na} would be due to the smaller cell body (Table 1, 'Membrane capacitance') and impaired neurite extension of R424H-expressing PCs. The expression of R424H mutant subunits did not affect the threshold current, threshold potential or action potential amplitude of PCs compared with expression of GFP (Fig. 6*E–G*). These results strongly suggest that expression of R424H mutant subunits inhibited the activation of the endogenous mKv3.3 channels, resulting in a reduction of the maximal rate of fall and then in the broadening of action potential duration in PCs.

We next examined the firing properties evoked by long current injection (200 ms duration). Most GFP-expressing PCs (82.9%) showed tonic firing of action potentials (tonic type) in response to depolarizing current injection (Fig. 7*A* and filled column of GFP in Fig. 7*E*), which is consistent with previous reports on the firing pattern of cultured PCs (Tabata *et al.* 2000; Harada *et al.* 2006). The other PCs (17.1%) showed a few spikes (up to three spikes) in response to current injection ranging from 0 to 200 pA

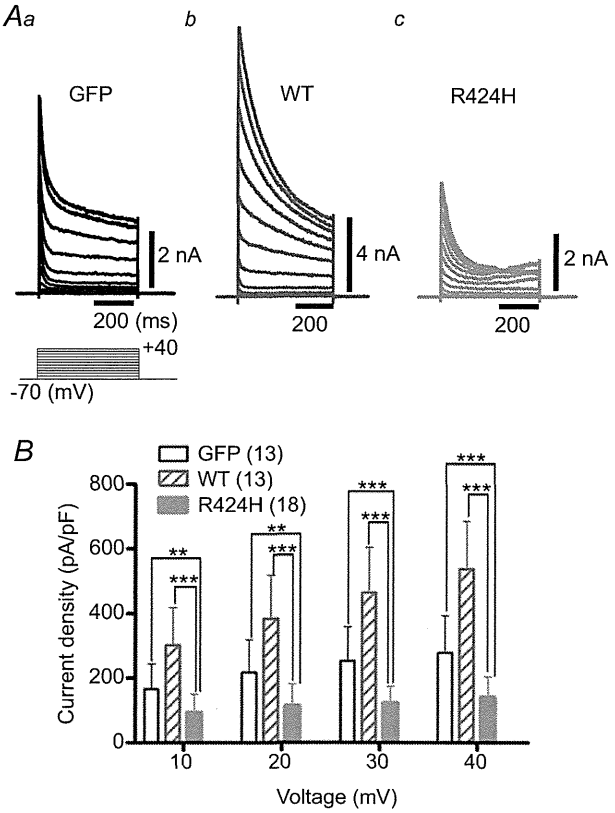

Figure 4. R424H mutant-expressing PCs exhibit suppressed peak outward current density
A, representative outward current traces recorded from PCs expressing GFP alone (*Aa*), WT subunits (*Ab*; note the vertical scale bar) and R424H mutant subunits (*Ac*). The currents were evoked by voltage steps from the −70 mV holding potential to voltages ranging from −60 to +40 mV in 10 mV increments. Leak currents were subtracted online by the *P*/4 protocol. The currents were recorded at DIV 8–10 in Hepes-buffered srtificial cerebrospinal fluid (ACSF) containing TTX, $CdCl_2$, picrotoxin and 6,7-dinitroquinoxaline-2,3-dione (DNQX). *B*, summary of the peak outward current density, which was calculated by dividing the peak outward current by membrane capacitance. $^{**}P < 0.01$ and $^{***}P < 0.001$.

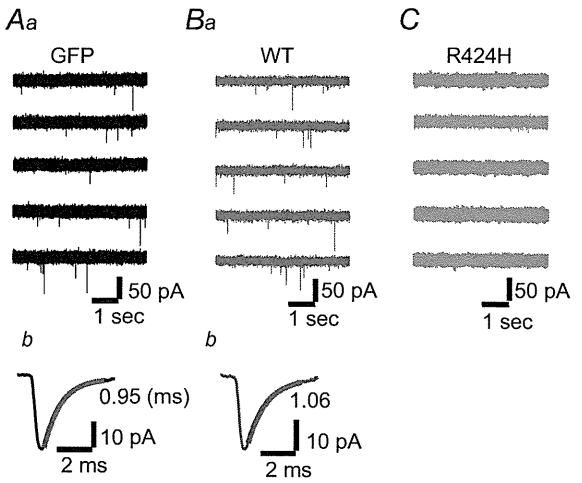

Figure 5. Absence of spontaneous excitatory postsynaptic currents (sEPSCs) in R424H mutant-expressing PCs
Aa, *Ba* and *C*, representative current traces recorded from PCs expressing GFP alone (*Aa*), WT subunits (*Ba*) or R424H mutant subunits (*C*). The sEPSCs appear as downward deflections in *Aa* and *Ba*. The PCs were held at −80 mV in the presence of picrotoxin. *Ab* and *Bb*, averaged sEPSCs from the same cell as in *Aa* and *Ba*, with superimposed single exponential fit. The decay time constant is indicated beside each trace.

Table 2. Summary of spontaneous excitatory postsynaptic current (sEPSC) properties in Purkinje cells

	Percentage of cells showing sEPSCs[a]	Amplitude (pA)[b]	Frequency (Hz)[b]	10–90% Rise time (ms)[b]	Decay time constant (ms)[c]
GFP alone	100%	33.7 ± 9.3	0.62 ± 0.35	0.18 ± 0.04	0.84 ± 0.27
(n = 15; 1502 events)	(15 of 15 cells)	(n = 15)	(n = 15)	(n = 15)	(n = 15)
WT mKv3.3	100%	34.0 ± 12.0	0.73 ± 0.35	0.19 ± 0.03	0.87 ± 0.19
(n = 10; 1041 events)	(10 of 10 cells)	(n = 10)	(n = 10)	(n = 10)	(n = 10)
R424H mutant	23%	23.1 ± 4.2	0.15 ± 0.10	0.20 ± 0.02	1.14 ± 0.21
(n = 3; 103 events)	(3 of 13 cells)**††	(n = 3)	(n = 3)*†	(n = 3)	(n = 3)

All measurements were performed at a holding potential of −80 mV. The statistical analyses indicated by superscript letters a and b were conducted using Student's unpaired t test and Fisher's exact probability test, respectively. [c]The sEPSC decay phases were fitted with a single exponential function. *P < 0.05, **P < 0.001 between GFP alone and R424H mutant. †P < 0.05, ††P < 0.001 between WT mKv3.3 and R424H mutant.

in 20 pA increments and did not fire tonically during the 200 ms depolarizing pulses (onset type; open column of GFP in Fig. 7*E*). However, approximately half of the R424H mutant-expressing PCs exhibited onset-type firing (53.6%; Fig. 7*C* and *E*), and the remaining PCs exhibited tonic-type firing (46.4%; Fig. 7*D* and *E*). The percentages of firing types in R424H mutant-expressing PCs differed significantly from those in GFP- and WT-expressing PCs (Fig. 7*E*; $P < 0.001$ in both pairs by the χ^2 test). The firing frequencies of tonic-type neurons in the three groups were plotted against the injected current (Fig. 7*F*). Wild-type-expressing PCs showed the highest frequencies, in the range of 40–200 pA (Fig. 7*B* and *F*), demonstrating that lentivirally expressed WT subunits contributed to the generation of narrow action potentials by accelerating the falling phase (Fig. 7*A* and *D* and Supplemental Fig. S3*E*). In tonic-type neurons, firing frequencies in R424H mutant-expressing PCs were significantly lower than those in GFP-expressing PCs, in the range of 180–200 pA (Fig. 7*F*; $P < 0.05$ at 180 and 200 pA depolarization). These results demonstrate that expression of R424H mutant subunits changed the ratio of tonic-firing PCs and reduced PC excitability in response to depolarization.

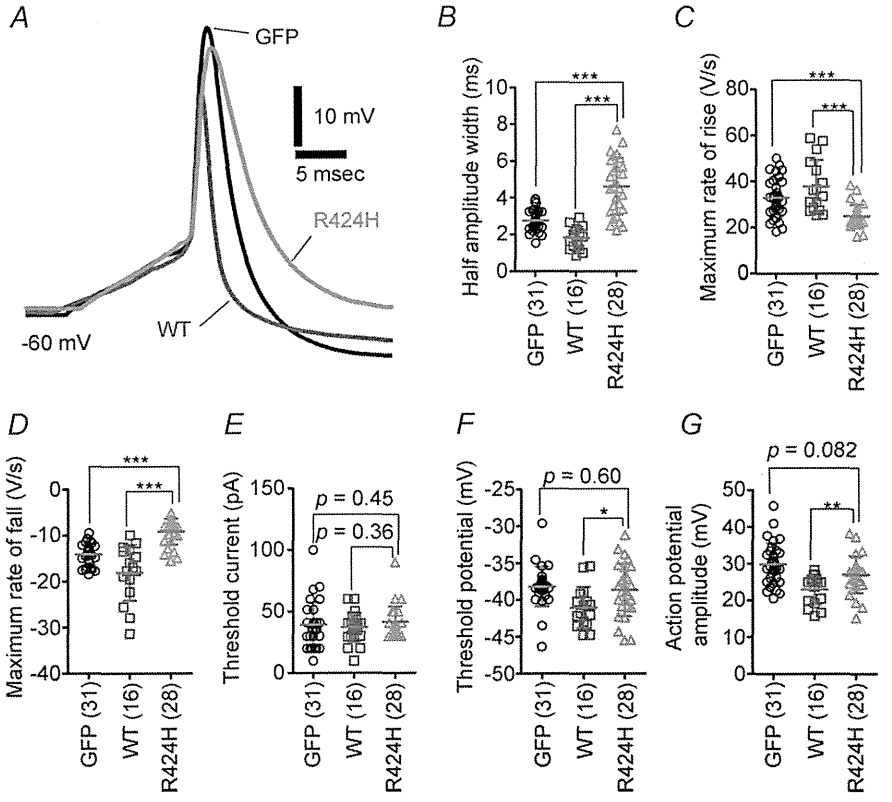

Figure 6. R424H mutant-expressing PCs exhibit broadened action potential waveforms
A, representative single action potential waveforms of PCs. The action potentials were evoked by short depolarizing current injection (10 ms duration). Action potentials were aligned by superimposing the rising phase of each trace. The resting membrane potentials were adjusted to −60 mV by current injection. *B*–*G*, comparison of action potential properties. *B*, half-amplitude width measured at the mid-point between the threshold and peak of the action potential. *C* and *D*, maximal rate of rise (*C*) and of fall (*D*) of action potentials. *E*, threshold current amplitude. *F*, threshold potential. *G*, action potential amplitude, as measured between the threshold and peak. *P < 0.05, **P < 0.01 and ***P < 0.001.

R424H mutant-expressing PCs show higher $[Ca^{2+}]_i$, and blockade of P/Q-type Ca^{2+} channels rescues the PC death and dendritic maldevelopment caused by the mutant subunits

The expression of R424H mutant subunits in cerebellar cultures caused PC death. We hypothesized that the cell death was caused by excessive Ca^{2+} influx through the following steps. As cultured PCs spontaneously generate action potentials, which increase basal $[Ca^{2+}]_i$ (Schilling *et al.* 1991; Supplemental Fig. S4*B* and *C* and Table 1), the broadening of action potentials by R424H mutant expression would cause increased Ca^{2+} influx via excessive activation of voltage-gated Ca^{2+} channels. This influx would lead to a defect of Ca^{2+} homeostasis in PCs, resulting in the cell death as a part of a stress response (Orrenius *et al.* 2003). Indeed, excessive Ca^{2+} influx triggered by the blockade of K^+ channels has been shown to induce cell death in several types of cells (Kim *et al.* 2000; Lajdova *et al.* 2004; Wang *et al.* 2011). To test this hypothesis, we performed calcium imaging (Fig. 8) and then rescue experiments of PC death using ω-agatoxin IVA, a specific blocker for the P/Q-type voltage-gated Ca^{2+} channels that mediate predominant Ca^{2+} currents in PCs (Mintz & Bean, 1993; Gillard *et al.* 1997; Fig. 9).

Calcium imaging was performed using cerebellar cultures loaded with fura-2 AM (see Methods). After a baseline recording (measurement of basal $[Ca^{2+}]_i$) for 8 min, cerebellar cultures were depolarized for 5 min by perfusion of high-K^+ ACSF (Fig. 8*B*). In basal conditions, $[Ca^{2+}]_i$ in R424H mutant-expressing PCs was approximately four times higher than in the control group (Fig. 8*Ca*; $P < 0.001$ in R424H *versus* GFP and in R424H *versus* WT). There were no significant differences in high-K^+-induced $[Ca^{2+}]_i$ elevation (~200 nM) between PCs expressing the R424H mutant and those expressing GFP alone or expressing WT subunits (Fig. 8*Cb*). The basal $[Ca^{2+}]_i$ of granule cells infected with the

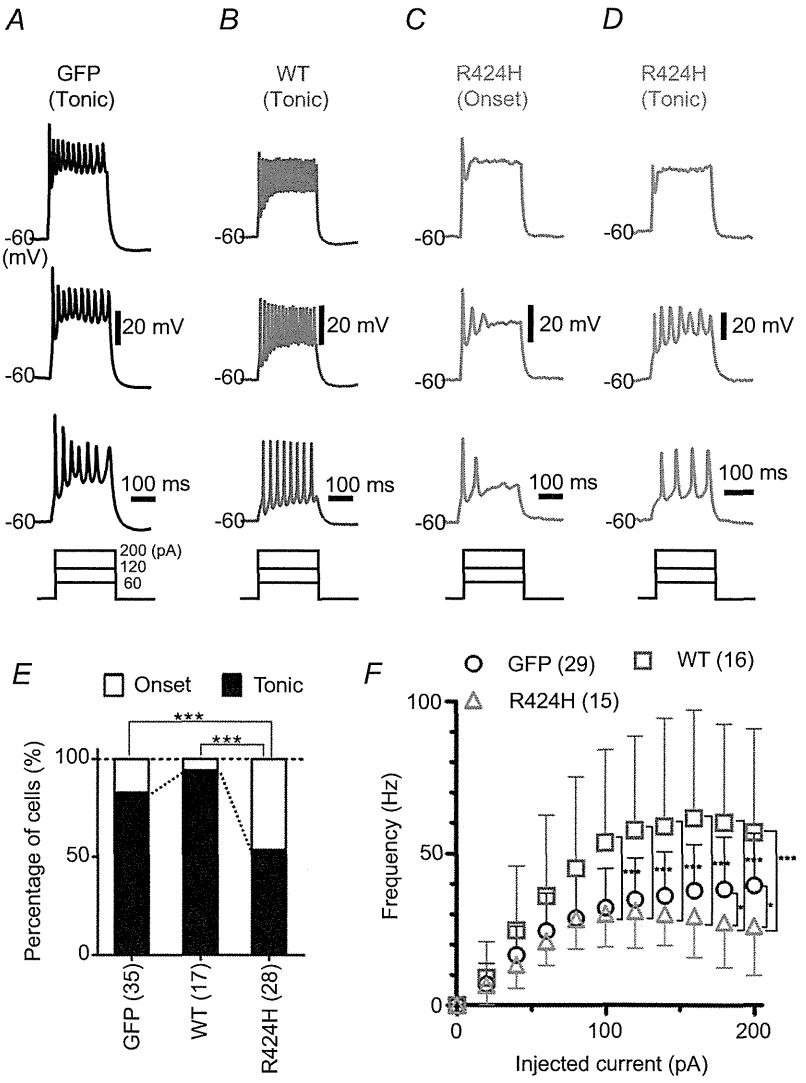

Figure 7. R424H mutant-expressing PCs exhibit altered firing patterns
A–D, representative firing patterns of PCs expressing GFP alone (*A*), WT subunits (*B*) or R424H mutant subunits (*C* and *D*). Approximately half of the R424H mutant-expressing PCs fired at the onset of current injection (onset-type; *C*). The action potentials were evoked by long depolarizing current injection (200 ms duration). The resting membrane potentials were adjusted to −60 mV. *E*, comparison of firing patterns. The χ^2 test was used for the statistical analyses. *F*, the firing frequency of the tonic-type cells is plotted as a function of injected current. $^*P < 0.05$ and $^{***}P < 0.001$.

lentiviruses was also measured, and there were no significant differences between R424H mutant-expressing and control cultures (GFP, 71.2 ± 41.2 nM, $n = 86$; WT, 69.7 ± 38.0 nM, $n = 118$; R424H, 63.6 ± 32.9 nM, $n = 72$; $P = 0.365$ between GFP and R424H; $P = 0.423$ between WT and R424H).

To examine whether the elevated basal $[Ca^{2+}]_i$ induced PC death in R424H mutant-expressing cultures, we performed a similar experiment to that in Fig. 2. In this experiment, ω-agatoxin IVA (0.2 μM) was added to the culture medium at DIV 2 (see Methods), and WT-expressing cultures were omitted to simplify the experimental design. Treatment of GFP-expressing cultures with ω-agatoxin IVA did not affect relative PC density (Fig. 9*D*, filled circles) but increased the branch number and the total length of dendrites at DIV 14 (Fig. 9*E* and *F*; filled circles in Fig. 9*I* and *J*), in good agreement with a previous report (Schilling *et al.* 1991; see Discussion). Treatment of R424H mutant-expressing cultures with ω-agatoxin IVA significantly increased relative PC density at DIV 11 and 14 (Fig. 9*D*, red triangles) and significantly rescued dendritic development in PCs (Fig. 9*G* and *H*; red triangles in Fig. 9*I* and *J*). These results clearly indicate that P/Q-type Ca^{2+} channels play a critical role in the PC death and impairment of dendrite development caused by R424H mutant expression, and support our hypothesis.

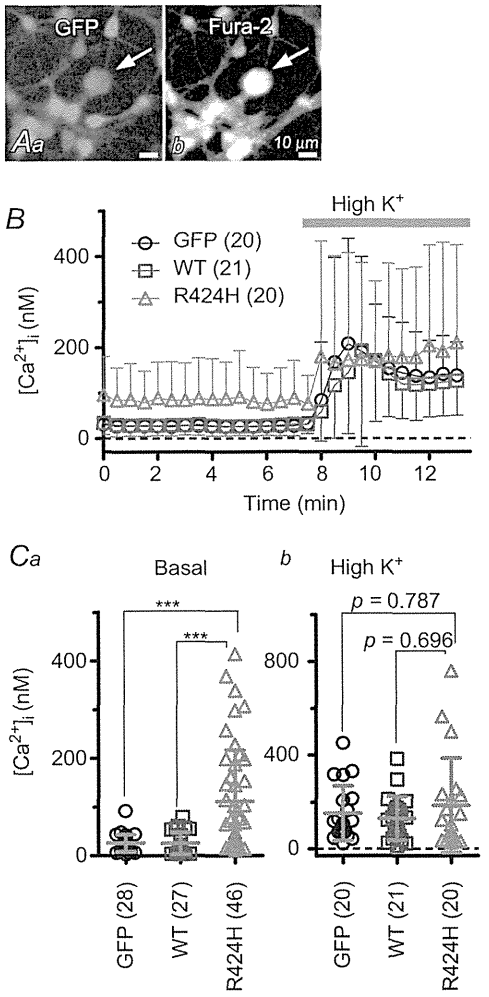

Figure 8. Significantly higher basal $[Ca^{2+}]_i$ in PCs expressing R424H mutant
A, representative fluorescence images of a fura-2 AM-loaded cerebellar culture expressing GFP alone. Arrows indicate PCs. *Aa*, GFP fluorescence (excitation, 470–495 nm; emission, 510–550 nm). *Ab*, fura-2 fluorescence (excitation, 375–385 nm; emission, 470–550 nm). *B*, the time course of free $[Ca^{2+}]_i$ in PCs. To depolarize PCs, high-K^+ ACSF (High K^+) was bath applied during the time indicated by the grey bar. *C*, summary of averaged $[Ca^{2+}]_i$ in PCs. Basal $[Ca^{2+}]_i$ was obtained as the average of a 7 min period from the beginning of the recordings (*Ca*), and elevated $[Ca^{2+}]_i$ from a 5 min period during high-K^+ ACSF perfusion (*Cb*). ***$P < 0.001$.

Discussion

In this study, we found that the expression of R424H mutant subunits in cerebellar cultures significantly impaired dendritic development and survival in PCs (Figs 2 and 3). Prior to cell death, R424H mutant-expressing PCs showed broadened action potential waveforms, altered firing properties and elevated basal $[Ca^{2+}]_i$ (Figs 6–8). Moreover, chronic inhibition of P/Q-type Ca^{2+} channels by ω-agatoxin IVA rescued the PC death and dendritic maldevelopment caused by expression of R424H mutant subunits (Fig. 9). This is the first report to show that a missense mutation found in SCA13 patients induces maldevelopment of PC dendrites and eventually PC death, most probably due to elevated basal $[Ca^{2+}]_i$ in PCs.

Biophysical properties of R424H mutant channels

The biophysical properties of hKv3.3 channels with the R423H mutation, which corresponds to the R424H mutation in mKv3.3 channels, have been previously reported (Figueroa *et al.* 2010; Minassian *et al.* 2012). Our results in Supplemental Fig. S2 agreed well with the previous reports and suggest that the properties of R424H mutant mKv3.3 were essentially identical to those of R423H-mutant hKv3.3. Moreover, we found that coexpression of R424H mutant and WT subunits accelerated the inactivation kinetics and slowed recovery from inactivation compared with expression of WT subunits alone (Fig. 1). Therefore, we predict that the properties we found in R424H mutant mKv3.3 are shared with R423H mutant hKv3.3.

We confirmed that homomeric R424H mutant channels showed negligible currents and that R424H mutant subunits exerted a dominant-negative influence on WT mKv3.3 channels in *Xenopus* oocytes (Supplemental Fig. S2*A* and *B*; Figueroa *et al.* 2010, 2011). Very recently,

Zhao *et al.* (2013) reported that in heterologous expression systems using Chinese hamster ovary cells, the surface protein level of R423H mutant hKv3.3 channels is 30% of that of WT hKv3.3 and that the conductance density of the mutant is 16% of that of the WT. Therefore, we cannot exclude the possibility that the reduced surface expression of mKv3.3 channels by the mutation would also contribute to the broadening of action potentials (Fig. 6) and lower firing frequency (Fig. 7) in transduced PCs. However, the reduction of the conductance density cannot be explained fully by the reduced surface protein expression.

To explain the negligible activity and dominant-negative property of R424H mutant channels, we propose two hypothetical mechanisms. First, the positively charged arginine at position 424 in mKv3.3 may be a critical residue in the S4 segment, serving as a part of the voltage sensor domain (Seoh *et al.* 1996). The partial disruption of the sensor domain by R424H mutation would make the subunits less sensitive to membrane voltage changes, resulting in the loss of channel function. Second, an arginine residue at position 174 in the S4 segment of KAT1, which is a voltage-gated K^+ channel in *Arabidopsis*, plays an essential role in the appropriate integration of the S3 and S4 segment into the endoplasmic reticulum membrane (Sato *et al.* 2003). Given that the R174 is homologous to R424 in mKv3.3, defective membrane insertion of R424H mutant subunits could occur in *Xenopus* oocytes, leading to a defect in channel activity.

Purkinje cell death by R424H mutant expression and the inhibition by blockade of P/Q-type voltage-gated Ca^{2+} channels

In this study, we revealed that expression of R424H mutant subunits caused cell death and impaired dendritic growth in PCs (Figs 2 and 3) and that these effects were reversed by the blockade of P/Q-type Ca^{2+} channels (Fig. 9). Addition of ω-agatoxin IVA also enhanced dendritic elongation in PCs expressing GFP alone (Fig. 9*E* and *F*; filled circles in Fig. 9*I* and *J*). Together with a previous report showing that chronic application of TTX in cerebellar cultures caused dendritic elongation in PCs (Schilling *et al.* 1991), activation of P/Q-type Ca^{2+} channels by neuronal activity may adversely influence dendritic elongation in PCs. Addition of ω-agatoxin IVA in R424H mutant-expressing cultures did not completely restore PC survival rates

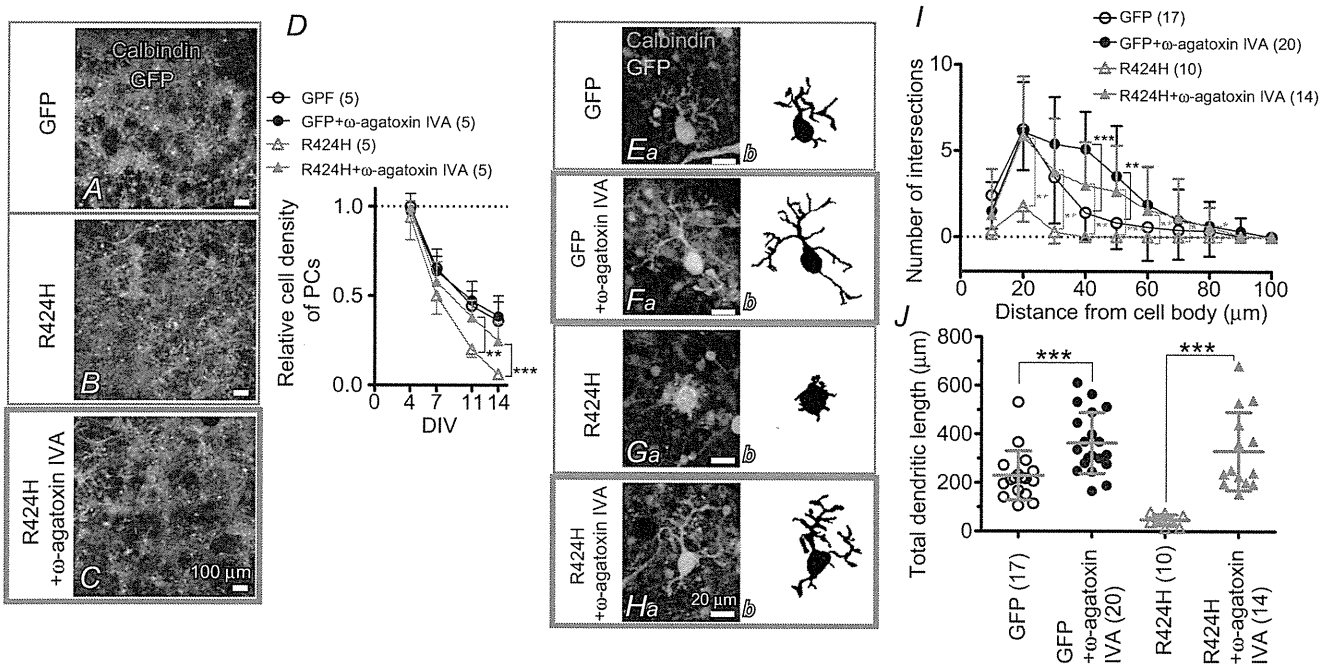

Figure 9. Pharmacological blockade of P/Q-type Ca^{2+} channels rescues the PC death and dendritic maldevelopment caused by expression of R424H mutant
A–C, cerebellar cultures expressing GFP alone (*A*) or R424H mutant with GFP (*B* and *C*). The cultures were immunostained for calbindin at DIV 14. In *C*, ω-agatoxin IVA was added to the culture medium every other day from DIV 2. *D*, relative cell density of PCs plotted as a function of DIV. The density was normalized to the value of PCs expressing GFP alone at DIV 4. *E–H*, calbindin-immunolabelled PCs expressing GFP alone (*Ea* and *Fa*) or R424H mutant subunits with GFP (*Ga* and *Ha*) at DIV 14. Morphologies of PCs are depicted in the right-hand panels for clarity. In *F* and *H*, ω-agatoxin IVA was added. *I*, and *J*, summary of dendrite complexity measured by Sholl analysis (*I*) and of total dendritic length (*J*). $^*P < 0.05$, $^{**}P < 0.01$, and $^{***}P < 0.001$.

(Fig. 9*D*). This may be because some Ca^{2+} currents in cultured PCs are mediated by Ca^{2+} channels other than the P/Q-type (Gillard *et al.* 1997), and activation of these channels may contribute to PC death. We therefore performed the same rescue experiments using $CdCl_2$ (0.2 mM; a non-selective Ca^{2+} channel blocker) or a combination of ω-agatoxin IVA and verapamil hydrochloride (0.02 mM; an L-type Ca^{2+} channel blocker), but these chemicals markedly deteriorated the viability and development of cerebellar cultures within 3 DIV (data not shown).

In contrast to PCs, there were no significant decreases in the numbers of granule cells upon R424H mutant expression (Fig. 2*E*). This may be because granule cells do not express endogenous mKv3.3 channels with which R424H mutant subunits form oligomeric channels (Supplemental Fig. S3*C*), resulting in the absence of the dominant-negative influence on the endogenous channels by the expression of mutant channel subunits.

Comparison with preceding papers on Kv3.3 knockout mice and zebrafish expressing mutant Kv3.3

In contrast to the impaired dendritic development in R424H mutant-expressing PCs (Fig. 3*Cb′* and *D*), the cerebellum of Kv3.3 knockout mice shows neither dendritic shrinkage of PCs nor cerebellar atrophy (Zagha *et al.* 2010). Furthermore, the knockout mice display only moderate motor dysfunction and no ataxic phenotype, although SCA13 patients show severe ataxia (Joho *et al.* 2006; Hurlock *et al.* 2008; Waters & Pulst, 2008; Figueroa *et al.* 2010). This difference may be attributable to the following factors. In PCs, mKv3.3 is thought to form heteromultimeric channels by assembling with Kv3.1 and/or Kv3.4 (Goldman-Wohl *et al.* 1994; Weiser *et al.* 1994), and Kv3 channels contribute to repolarization of both somatic Na^+ spikes and dendritic Ca^{2+} spikes (McKay & Turner, 2004). Genetic elimination of Kv3.3 subunits may be insufficient to exhibit the dendritic shrinkage and severe ataxia phenotypes because of functional compensation by Kv3.1 and Kv3.4 in PCs (Goldman-Wohl *et al.* 1994; Weiser *et al.* 1994; Martina *et al.* 2003). We detected the expression of Kv3.4 subunits in cultured PCs (Supplemental Fig. S3*D*). It is therefore reasonable to hypothesize that R424H mutant subunits form heteromultimeric channels not only with endogenous mKv3.3 but also with other members of Kv3.3, including Kv3.4, resulting in total inhibition of the K^+ channel activity in PCs. This may account for the differences in the morphological phenotypes of PCs in our results *versus* the knockout mice.

Zebrafish expressing infant-onset mutant zebrafish Kv3.3 (homologous to the F448L mutant in SCA13 patients) in spinal motoneurons show defective axonal pathfinding (Issa *et al.*, 2012). Indeed, the zebrafish is an interesting model for understanding the effects of mutant Kv3.3 expression in spinal motoneurons. However, as they used a motoneuron-specific enhancer of *Mnx1* (*Hb9*) gene, the exogenous proteins were not expressed in the cerebellar neurons. To examine the effects of mutant Kv3.3 in the cerebellum, it would be necessary to express the mutant protein directly in the cerebellar neurons using a different method.

Comparison of our culture results with SCA13 patients harbouring the R423H mutation

Spinocerebellar ataxia type 13 patients harbouring the R423H mutation generally show early-onset, slow-progressive ataxia and cerebellar atrophy (Figueroa *et al.* 2010, 2011). Our immunohistochemical analyses demonstrated that expression of R424H mutant subunits impaired dendritic development and induced cell death in cultured PCs (Figs 2 and 3). Those defects may be responsible for the cerebellar atrophy and ataxia observed in SCA13 patients, although it is necessary to verify that similar impairments are also observed in post-mortem cerebellum of the patients.

In functional aspects, we found that expression of R424H mutant subunits significantly decreased outward current mediated by voltage-gated K^+ channels, reduced sEPSCs, broadened action potentials and altered firing properties (Figs 4–7 and Table 2), suggesting the existence of similar functional changes in SCA13 patients. As PCs are the sole output neurons from the cerebellar cortex and make inhibitory synaptic contacts directly onto neurons in the deep cerebellar nuclei and the vestibular nuclei in the brainstem, PCs play crucial roles in motor co-ordination (Zheng & Raman, 2010). Accordingly, it is easily assumed that the reduction of spontaneous excitatory inputs and the changed firing properties in PCs disrupt synaptic transmission to neurons in the deep cerebellar nuclei and vestibular nuclei, resulting in impaired motor co-ordination. To examine the effects of the R424H mutation on electrophysiological properties of PCs and animal behaviour, we tried expressing R424H mutant subunits in PCs *in vivo* by directly injecting the virus solution into mouse cerebellar cortex as described in our previous papers (Torashima *et al.* 2006, 2008; Shuvaev *et al.* 2011). However, despite the presence of the infection, sufficient overexpression of mKv3.3 channels and apparent ataxia were not observed (data not shown). This may be because endogenous mKv3.3 proteins are abundantly expressed in PCs and the overexpression failed to reach the endogenous protein level. Efficient reduction of K^+ currents in PCs *in vivo* as observed in cultured PCs may be attained by using a different type of viral vector, such as adeno-associated virus vectors (Nathanson *et al.* 2009). Alternatively, K^+ currents in PCs *in vivo* may be effectively decreased using viral vector-mediated

expressions of R424H mutant subunits in *Kv3.3*$^{-/-}$ or *Kv3.3*$^{+/-}$ mice, which express no mKv3.3 proteins or only half the normal amount.

Currently, three different missense mutations in hKv3.3 channels have been reported from distinct pedigrees, and the disease onset and clinical phenotypes also differ among them (Waters *et al.* 2006; Figueroa *et al.* 2010, 2011). In the present study, we focused on only one mutation (R423H in hKv3.3) because of the drastic changes it induced in channel properties in the *Xenopus* oocyte expression system and its early-onset phenotype in SCA13 patients. Further studies of the effects of other mutants (R420H and F448L in hKv3.3) on cultured PCs may provide explanations for the differences in the disease phenotypes.

Possible significance of this study

We developed an *in vitro* SCA13 model using mouse cerebellar cultures and lentivirus vector-mediated gene expression. This model has advantages over *in vivo* models, such as transgenic mice, in the ease of controlling culture conditions by applying chemical compounds. Therefore, this model would be useful in screening drugs for SCA13 and in detailed investigations of the signalling cascades that promote the observed cell death. Given that blockade of P/Q-type Ca^{2+} channels rescued the phenotypes found in this research, the channel blockers may be potential therapeutic drugs for SCA13. Furthermore, this culture method, in combination with virus-mediated gene expression, may be applicable to the study of other types of hereditary spinocerebellar ataxia.

References

Armstrong CM & Bezanilla F (1974). Charge movement associated with the opening and closing of the activation gates of the Na channels. *J Gen Physiol* **63**, 533–552.

Ashcroft FM (2006). From molecule to malady. *Nature* **440**, 440–447.

Chang SY, Zagha E, Kwon ES, Ozaita A, Bobik M, Martone ME, Ellisman MH, Heintz N & Rudy B (2007). Distribution of Kv3.3 potassium channel subunits in distinct neuronal populations of mouse brain. *J Comp Neurol* **502**, 953–972.

Costa PF, Emilio MG, Fernandes PL, Ferreira HG & Ferreira KG (1989). Determination of ionic permeability coefficients of the plasma membrane of *Xenopus laevis* oocytes under voltage clamp. *J Physiol* **413**, 199–211.

Desai R, Kronengold J, Mei J, Forman SA & Kaczmarek LK (2008). Protein kinase C modulates inactivation of Kv3.3 channels. *J Biol Chem* **283**, 22283–22294.

Drummond GB (2009). Reporting ethical matters in *The Journal of Physiology*: standards and advice. *J Physiol* **587**, 713–719.

Erisir A, Lau D, Rudy B & Leonard CS (1999). Function of specific K^+ channels in sustained high-frequency firing of fast-spiking neocortical interneurons. *J Neurophysiol* **82**, 2476–2489.

Figueroa KP, Minassian NA, Stevanin G, Waters M, Garibyan V, Forlani S, Strzelczyk A, Bürk K, Brice A, Dürr A, Papazian DM & Pulst SM (2010). KCNC3: phenotype, mutations, channel biophysics—a study of 260 familial ataxia patients. *Hum Mutat* **31**, 191–196.

Figueroa KP, Waters MF, Garibyan V, Bird TD, Gomez CM, Ranum LP, Minassian NA, Papazian DM & Pulst SM (2011). Frequency of KCNC3 DNA variants as causes of spinocerebellar ataxia 13 (SCA13). *PLoS One* **6**, e17811.

Fry M, Boegle AK & Maue RA (2007). Differentiated pattern of sodium channel expression in dissociated Purkinje neurons maintained in long-term culture. *J Neurochem* **101**, 737–748.

Gillard SE, Volsen SG, Smith W, Beattie RE, Bleakman D & Lodge D (1997). Identification of pore-forming subunit of P-type calcium channels: an antisense study on rat cerebellar Purkinje cells in culture. *Neuropharmacology* **36**, 405–409.

Gimenez-Cassina A, Lim F & Diaz-Nido J (2007). Gene transfer into Purkinje cells using herpesviral amplicon vectors in cerebellar cultures. *Neurochem Int* **50**, 181–188.

Goldman-Wohl DS, Chan E, Baird D & Heintz N (1994). Kv3.3b: a novel Shaw type potassium channel expressed in terminally differentiated cerebellar Purkinje cells and deep cerebellar nuclei. *J Neurosci* **14**, 511–522.

Grynkiewicz G, Poenie M & Tsien RY (1985). A new generation of Ca^{2+} indicators with greatly improved fluorescence properties. *J Biol Chem* **260**, 3440–3450.

Hanawa H, Hematti P, Keyvanfar K, Metzger ME, Krouse A, Donahue RE, Kepes S, Gray J, Dunbar CE, Persons DA & Nienhuis AW (2004). Efficient gene transfer into rhesus repopulating hematopoietic stem cells using a simian immunodeficiency virus-based lentiviral vector system. *Blood* **103**, 4062–4069.

Harada KH, Ishii TM, Takatsuka K, Koizumi A & Ohmori H (2006). Effects of perfluorooctane sulfonate on action potentials and currents in cultured rat cerebellar Purkinje cells. *Biochem Biophys Res Commun* **351**, 240–245.

Hawley RG, Lieu FH, Fong AZ & Hawley TS (1994). Versatile retroviral vectors for potential use in gene therapy. *Gene Ther* **1**, 136–138.

Hille B (2001). *Ion Channels of Excitable Membranes*. Sinauer, Sunderland, MA.

Hirai H & Launey T (2000). The regulatory connection between the activity of granule cell NMDA receptors and dendritic differentiation of cerebellar Purkinje cells. *J Neurosci* **20**, 5217–5224.

Hirano T & Kasono K (1993). Spatial distribution of excitatory and inhibitory synapses on a Purkinje cell in a rat cerebellar culture. *J Neurophysiol* **70**, 1316–1325.

Hirano T, Kubo Y & Wu MM (1986). Cerebellar granule cells in culture: monosynaptic connections with Purkinje cells and ionic currents. *Proc Natl Acad Sci U S A* **83**, 4957–4961.

Hodgkin AL & Katz B (1949). The effect of sodium ions on the electrical activity of giant axon of the squid. *J Physiol* **108**, 37–77.

Hurlock EC, McMahon A & Joho RH (2008). Purkinje-cell-restricted restoration of Kv3.3 function restores complex spikes and rescues motor coordination in *Kcnc3* mutants. *J Neurosci* **28**, 4640–4648.

Issa FA, Mock AF, Sagasti A & Papazian DM (2012). Spinocerebellar ataxia type 13 mutation that is associated with disease onset in infancy disrupts axonal pathfinding during neuronal development. *Dis Model Mech* **5**, 921–929.

Joho RH, Street C, Matsushita S & Knöpfel T (2006). Behavioral motor dysfunction in Kv3-type potassium channel-deficient mice. *Genes Brain Behav* **5**, 472–482.

Kim JA, Kang YS, Jung MW, Kang GH, Lee SH & Lee YS (2000). Ca^{2+} influx mediates apoptosis induced by 4-aminopyridine, a K^+ channel blocker, in HepG2 human hepatoblastoma cells. *Pharmacology* **60**, 74–81.

Kubo Y & Murata Y (2001). Control of rectification and permeation by two distinct sites after the second transmembrane region in Kir2.1 K^+ channel. *J Physiol* **531**, 645–660.

Lajdova I, Chorvat D Jr, Spustova V & Chorvatova A (2004). 4-Aminopyridine activates calcium influx through modulation of the pore-forming purinergic receptor in human peripheral blood mononuclear cells. *Can J Physiol Pharmacol* **82**, 50–56.

McKay BE & Turner RW (2004). Kv3 K^+ channels enable burst output in rat cerebellar Purkinje cells. *Eur J Neurosci* **20**, 729–739.

MacKinnon R (1991). Determination of the subunit stoichiometry of a voltage-activated potassium channel. *Nature* **350**, 232–235.

Martina M, Yao GL & Bean BP (2003). Properties and functional role of voltage-dependent potassium channels in dendrites of rat cerebellar Purkinje neurons. *J Neurosci* **23**, 5698–5707.

Mellor JR, Merlo D, Jones A, Wisden W & Randall AD (1998). Mouse cerebellar granule cell differentiation: electrical activity regulates the $GABA_A$ receptor $\alpha 6$ subunit gene. *J Neurosci* **18**, 2822–2833.

Mikuni T, Uesaka N, Okuno H, Hirai H, Deisseroth K, Bito H & Kano M (2013). Arc/Arg3.1 is a postsynaptic mediator of activity-dependent synapse elimination in the developing cerebellum. *Neuron* **78**, 1024–1035.

Minassian NA, Lin MC & Papazian DM (2012). Altered Kv3.3 channel gating in early-onset spinocerebellar ataxia type 13. *J Physiol* **590**, 1599–1614.

Mintz IM & Bean BP (1993). Block of calcium channels in rat neurons by synthetic omega-Aga-IVA. *Neuropharmacology* **32**, 1161–1169.

Mullen RJ, Buck CR & Smith AM (1992). NeuN, a neuronal specific nuclear protein in vertebrates. *Development* **116**, 201–211.

Nathanson JL, Yanagawa Y, Obata K & Callaway EM (2009). Preferential labelling of inhibitory and excitatory cortical neurons by endogenous tropism of adeno-associated virus and lentivirus vectors. *Neuroscience* **161**, 441–450.

Orrenius S, Zhivotovsky B & Nicotera P (2003). Regulation of cell death: the calcium–apoptosis link. *Nat Rev Mol Cell Biol* **4**, 552–565.

Rae JL & Shepard AR (2000). Kv3.3 potassium channels in lens epithelium and corneal endothelium. *Exp Eye Res* **70**, 339–348.

Rudy B & McBain CJ (2001). Kv3 channels: voltage-gated K^+ channels designed for high-frequency repetitive firing. *Trends Neurosci* **24**, 517–526.

Sato M, Suzuki K, Yamazaki H & Nakanishi S (2005). A pivotal role of calcineurin signalling in development and maturation of postnatal cerebellar granule cells. *Proc Natl Acad Sci U S A* **102**, 5874–5879.

Sato Y, Sakaguchi M, Goshima S, Nakamura T & Uozumi N (2003). Molecular dissection of the contribution of negatively and positively charged residues in S2, S3, and S4 to the final membrane topology of the voltage sensor in the K^+ channel, KAT1. *J Biol Chem* **278**, 13227–13234.

Sawada Y, Kajiwara G, Iizuka A, Takayama K, Shuvaev AN, Koyama C & Hirai H (2010). High transgene expression by lentiviral vectors causes maldevelopment of Purkinje cells in vivo. *Cerebellum* **9**, 291–302.

Schilling K, Dickinson MH, Connor JA & Morgan JI (1991). Electrical activity in cerebellar cultures determines Purkinje cell dendritic growth patterns. *Neuron* **7**, 891–902.

Seoh SA, Sigg D, Papazian DM & Bezanilla F (1996). Voltage-sensing residues in the S2 and S4 segments of the *Shaker* K^+ channel. *Neuron* **16**, 1159–1167.

Sholl DA (1953). Dendritic organization in the neurons of the visual and motor cortices of the cat. *J Anat* **87**, 387–406.

Shuvaev AN, Horiuchi H, Seki T, Goenawan H, Irie T, Iizuka A, Sakai N & Hirai H (2011). Mutant PKCγ in spinocerebellar ataxia type 14 disrupts synapse elimination and long-term depression in Purkinje cells *in vivo*. *J Neurosci* **31**, 14324–14334.

Szymczak AL, Workman CJ, Wang Y, Vignali KM, Dilioglou S, Vanin EF & Vignali DA (2004). Correction of multi-gene deficiency in vivo using a single 'self-cleaving' 2A peptide-based retroviral vector. *Nat Biotechnol* **22**, 589–594.

Tabata T, Sawada S, Araki K, Bono Y, Furuya S & Kano M (2000). A reliable method for culture of dissociated mouse cerebellar cells enriched for Purkinje neurons. *J Neurosci Methods* **104**, 45–53.

Takayama K, Torashima T, Horiuchi H & Hirai H (2008). Purkinje-cell-preferential transduction by lentiviral vectors with the murine stem cell virus promoter. *Neurosci Lett* **443**, 7–11.

Torashima T, Iizuka A, Horiuchi H, Mitsumura K, Yamasaki M, Koyama C, Takayama K, Iino M, Watanabe M & Hirai H (2009). Rescue of abnormal phenotypes in $\delta 2$ glutamate receptor-deficient mice by the extracellular N-terminal and intracellular C-terminal domains of the $\delta 2$ glutamate receptor. *Eur J Neurosci* **30**, 355–365.

Torashima T, Koyama C, Iizuka A, Mitsumura K, Takayama K, Yanagi S, Oue M, Yamaguchi H & Hirai H (2008). Lentivector-mediated rescue from cerebellar ataxia in a mouse model of spinocerebellar ataxia. *EMBO Rep* **9**, 393–399.

Torashima T, Okoyama S, Nishizaki T & Hirai H (2006). In vivo transduction of murine cerebellar Purkinje cells by HIV-derived lentiviral vectors. *Brain Res* **1082**, 11–22.

Wang W, Xiao J, Adachi M, Liu Z & Zhou J (2011). 4-Aminopyridine induces apoptosis of human acute myeloid leukemia cells via increasing $[Ca^{2+}]_i$ through P_2X_7 receptor pathway. *Cell Physiol Biochem* **28**, 199–208.

Waters MF, Minassian NA, Stevanin G, Figueroa KP, Bannister JP, Nolte D, Mock AF, Evidente VG, Fee DB, Müller U, Dürr A, Brice A, Papazian DM & Pulst SM (2006). Mutations in voltage-gated potassium channel KCNC3 cause degenerative and developmental central nervous system phenotypes. *Nat Genet* **38**, 447–451.

Waters MF & Pulst SM (2008). SCA13. *Cerebellum* **7**, 165–169.

Weiser M, Vega-Saenz de Miera E, Kentros C, Moreno H, Franzen L, Hillman D, Baker H & Rudy B (1994). Differential expression of Shaw-related K^+ channels in the rat central nervous system. *J Neurosci* **14**, 949–972.

Zagha E, Manita S, Ross WN & Rudy B (2010). Dendritic Kv3.3 potassium channels in cerebellar Purkinje cells regulate generation and spatial dynamics of dendritic Ca^{2+} spikes. *J Neurophysiol* **103**, 3516–3525.

Zhao J, Zhu J & Thornhill WB (2013). Spinocerebellar ataxia-13 Kv3.3 potassium channels: arginine-to-histidine mutations affect both functional and protein expression on the cell surface. *Biochem J* **454**, 259–265.

Zheng N & Raman IM (2010). Synaptic inhibition, excitation, and plasticity in neurons of the cerebellar nuclei. *Cerebellum* **9**, 56–66.

Additional Information

Competing interests

None declared.

Author contributions

T.I. and H.H. conceived and designed experiments. T.I. and Y.M. performed experiments. T.I. collected and analysed data. T.I., Y.S. and H.H. wrote the paper.

Funding

This work was supported by Health Labour Sciences Research Grant (T.I.), JSPS KAKENHI grant numbers 24790230 (T.I.) and 19670003 (H.H.), and JSPS Funding Program for Next Generation World-Leading Researchers (LS021 to H.H.).

Acknowledgements

The lentiviral vector and MSCV promoter were provided by St Jude Children's Research Hospital and the American National Red Cross, respectively. We thank Dr L. K. Kaczmarek for mouse Kv3.3 cDNA and Dr K. Nakajo for technical advice and valuable comments on electrophysiological recording from *Xenopus* oocytes.

Journal of Pharmacological Sciences 127 (2015) 145–149

Contents lists available at ScienceDirect

Journal of Pharmacological Sciences

journal homepage: www.elsevier.com/locate/jphs

Short communication

Paroxetine prevented the down-regulation of astrocytic L-Glu transporters in neuroinflammation

Koki Fujimori [a, b], Junpei Takaki [a, b], Yukari Shigemoto-Mogami [a], Yuko Sekino [a], Takeshi Suzuki [b], Kaoru Sato [a, *]

[a] Laboratory of Neuropharmacology, Division of Pharmacology, National Institute of Health Sciences, 1-18-1 Kamiyoga, Setagaya-ku, Tokyo 158-8501, Japan
[b] Division of Basic Biological Science, Faculty of Pharmacy, Keio University, 1-5-30 Shiba-koen, Minato-ku, Tokyo 105-8512, Japan

ARTICLE INFO

Article history:
Received 4 August 2014
Received in revised form
26 August 2014
Accepted 18 September 2014
Available online 2 October 2014

Keywords:
Paroxetine
L-glutamate
Inflammation

ABSTRACT

The extracellular L-glutamate (L-Glu) concentration is elevated in neuroinflammation, thereby causing excitotoxicity. One of the mechanisms is down-regulation of astrocyte L-Glu transporters. Some antidepressants have anti-inflammatory effects. We therefore investigated effects of various antidepressants on the down-regulation of astrocyte L-Glu transporters in the in vitro neuroinflammation model. Among these antidepressants, only paroxetine was effective. We previously demonstrated that the down-regulation of astrocyte L-Glu transporters was caused by L-Glu released from activated microglia. We here clarified that only paroxetine inhibited L-Glu release from microglia. This is the novel action of paroxetine, which may bring advantages on the therapy of neuroinflammation.

Increasing evidence indicates that inflammatory processes play important roles in the pathogenesis of many neurodegenerative disorders (1–3). Under the neuroinflammatory conditions, it is known that the extracellular concentration of L-glutamate (L-Glu) and inflammatory mediators, such as proinflammatory cytokines, prostaglandins, free radicals and complements are elevated (4). L-Glu is one of the most abundant excitatory neurotransmitters in the mammalian CNS. The released L-Glu is immediately uptaken by astrocyte L-Glu transporters, GLAST (EAAT1 in human) and GLT-1 (EAAT2 in human), or sustained elevation of extracellular concentration of L-Glu induce excitotoxicity. The impairment of the astrocyte L-Glu transporters is reported in various neurological disorders including Alzheimer's disease (5), Parkinson's diseases (6) and amyotrophic lateral sclerosis (7). We found that the expression level of L-Glu transporters in astrocytes of astrocyte-microglia-neuron mixed culture was decreased in the *in vitro* model of the early stage of inflammation in the previous study (8). We clarified the interaction between astrocytes and microglia underlie the down-regulation of L-Glu transporters, i.e., activated microglia release L-Glu and the resulting elevation of extracellular L-Glu cause down-regulation of astrocytic L-Glu transporters. Some antidepressants are known to have anti-inflammatory effects (9, 10). In this study, therefore, we investigated the effects of various antidepressants on the decrease in the astrocytic L-Glu transporter function in the early stage of inflammation and the contribution of microglia to the effects.

Astrocyte-microglia-neuron mixed culture and microglia culture were performed according to the methods previously described (8). Antidepressants and serotonin (5-HT) were dissolved in PBS at 100 μM and 10 mM, respectively, and were diluted with culture medium at the time of use. At 8 DIV, the astrocyte-microglia-neuron mixed culture was treated with 10 ng/mL LPS for 72 h. Antidepressants were applied from 1 h before to the end of the LPS-treatment. Then the concentration of the L-Glu remaining in the culture medium 30 min after changing extracellular concentration of L-Glu to 100 μM was measured. The measurement of the extracellular L-Glu concentration in the medium was performed according to the methods previously described (8). Real-Time Quantitative RT-PCR, Western blotting, immunocytochemistry were also performed according to the methods previously

Abbreviations: ATP, adenosine 5′-triphosphate; CNS, central nervous system; DIV, days *in vitro*; GABA, γ-aminobutyric acid; L-glu, L-glutamate; LPS, lipopolysaccharide; PBS, phosphate-buffered saline; $P2X_4$, P2X prinoceptor 4; RNA, ribonucleic acid; SD, Sprague-Dawley; SDS, sodium dodecyl sulfate; SNRI, serotonin–norepinephrine reuptake inhibitor; SSRI, selective serotonin reuptake inhibitor; TCA, tricyclic antidepressant; 5-HT, 5-hydroxytryptamine.

* Corresponding author. Tel./fax: +81 3 3700 9698.
E-mail address: kasato@nihs.go.jp (K. Sato).

Peer review under responsibility of Japanese Pharmacological Society.

http://dx.doi.org/10.1016/j.jphs.2014.09.002

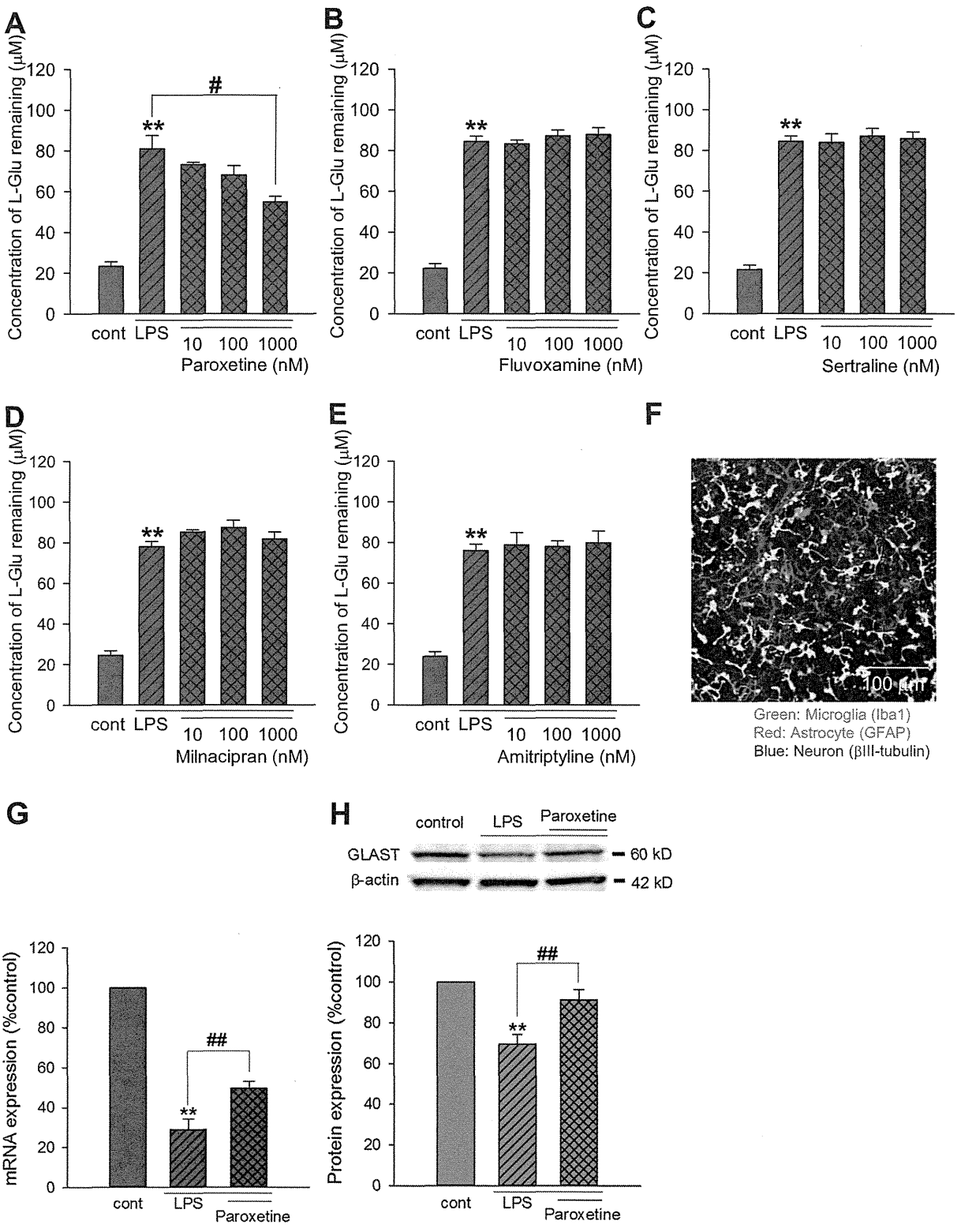

Fig. 1. Effects of antidepressants on the decreased L-Glu transport activity under the inflammatory condition. A–E. Antidepressants were applied to the mixed culture from 1 h before to the end of the LPS-treatment (10 ng/ml, 72 h). L-Glu transport activity was quantified as the L-Glu remaining 30 min after changing the extracellular concentration to 100 μM. Paroxetine prevented the LPS-induced decrease in the L-Glu transport activity in a concentration-dependent manner (A). Fluvoxamine (B), sertraline (C), milnacipran (D), and amitriptyline (E) had no effects. **: $p < 0.01$ vs. control group, #: $p < 0.05$ vs. LPS-treated group, Tukey's test following ANOVA ($N = 6$). F. Typical image of the microglia-astrocyte-neuron mixed culture immunostained with cell type-specific markers (Iba1: microglia; GFAP: astrocytes; βIII tubulin: neurons). G, H. Effects of paroxetine on the expression level of GLAST. Mixed cultures were treated with LPS (10 ng/ml) in the absence or presence of the paroxetine for 24 h (for mRNA level quantification) or 72 h (for protein level quantification). The expression level of GLAST was quantified at mRNA level (G) and protein level (H). LPS (10 ng/ml) caused significant decrease in GLAST mRNA level and paroxetine significantly prevented the decrease (G). LPS (10 ng/ml) caused significant decrease in GLAST protein level and paroxetine almost completely prevented the decrease (H). **: $p < 0.01$ vs. control group, ##: $p < 0.01$ vs. LPS-treated group, Tukey's test following ANOVA ($N = 5$).

described (8). The microglia culture was treated with LPS for 24 h in the presence or absence of antidepressants and the concentration of L-Glu in the medium was measured. All sets of the experiments were repeated in triplicate. All procedures described above were in accordance with institutional guidelines.

In the previous report, we showed that the expression level of astrocytic L-Glu transporters was decreased in the astrocyte-microglia-neuron mixed culture in LPS (10 ng/ml, 72 h)-induced inflammation model without cell death (8). We first compared the effects of various groups of antidepressants, i.e., selective serotonin reuptake inhibitors (SSRIs) (paroxetine, fluvoxamine, and sertraline), serotonin–norepinephrine reuptake inhibitor (SNRI) (milnacipran), and tricyclic antidepressant (TCA) (amitriptyline), on the decrease in the astrocytic L-Glu transporter function in this inflammation model. To quantify L-Glu transport activity, we measured the concentration of L-Glu remaining 30 min after changing the medium to the one containing 100 μM of L-Glu. In each set of experiment, LPS-induced decrease in the L-Glu transport activity was stably reproduced (Fig. 1A–E). Among antidepressants, only paroxetine prevented the LPS-induced decrease in L-Glu transport activity (Fig. 1A). The effect was concentration-dependent and reached significant at 1 μM. The other antidepressants had no effects (Fig. 1B–E). Typical image of the astrocyte-microglia-neuron mixed culture was shown in Fig. 1F. We have clarified that LPS-induced decrease in L-Glu transport activity was caused by the decrease in the expression level of GLAST, a predominant L-Glu transporter in the mixed culture, in both of mRNA and protein levels (8). In this study, LPS-induced decreases in the expression of GLAST, were reproduced at both of mRNA ($28.8 \pm 4.7\%$ of the control) and protein ($69.5 \pm 4.7\%$ of the control) levels (Fig. 1G, H). We then examined the effects of paroxetine on the LPS-induced decrease in the L-Glu transporter expression. Paroxetine significantly prevented the decreases at both of mRNA (28.8 ± 4.7 to $49.6 \pm 3.3\%$; $n = 10$) and protein (from $69.5 \pm 4.7\%$ to $91.0 \pm 5.1\%$; $n = 5$) levels (Fig. 1G, H). As is shown in Fig. 1, fluvoxamine and sertraline, the other SSRIs in this study, did not affect the decrease in L-Glu transport activity, suggesting that paroxetine revealed the effects through the mechanisms independent of its inhibitory effect on serotonin selective transporter. In support of this, LPS-induced decrease in L-Glu transport activity was not changed by the elevation of extracellular serotonin concentration (Fig. 2A). We also confirmed that paroxetine did not directly affect the L-Glu transport activity of the astrocyte culture (Fig. 2B). In our previous report, the down-regulation of GLAST in the inflammation model was caused by the elevation of extracellular L-Glu released from microglia (8). We therefore compared the effects of the antidepressants on LPS-induced L-Glu release from microglia. When microglia culture was treated with 10 ng/ml LPS for 24 h in the presence or absence of the antidepressants, only paroxetine suppressed L-Glu release in a concentration-dependent manner (Fig. 3A). The other antidepressants had no effects (Fig. 3B–E). We confirmed that paroxetine did not affect the microglial viability until 10 μM by LDH assay (data not shown). These results strongly suggest that the protective effect of paroxetine on the LPS-induced down-regulation of astrocytic L-Glu transporters was caused by the suppression of L-Glu release from microglia.

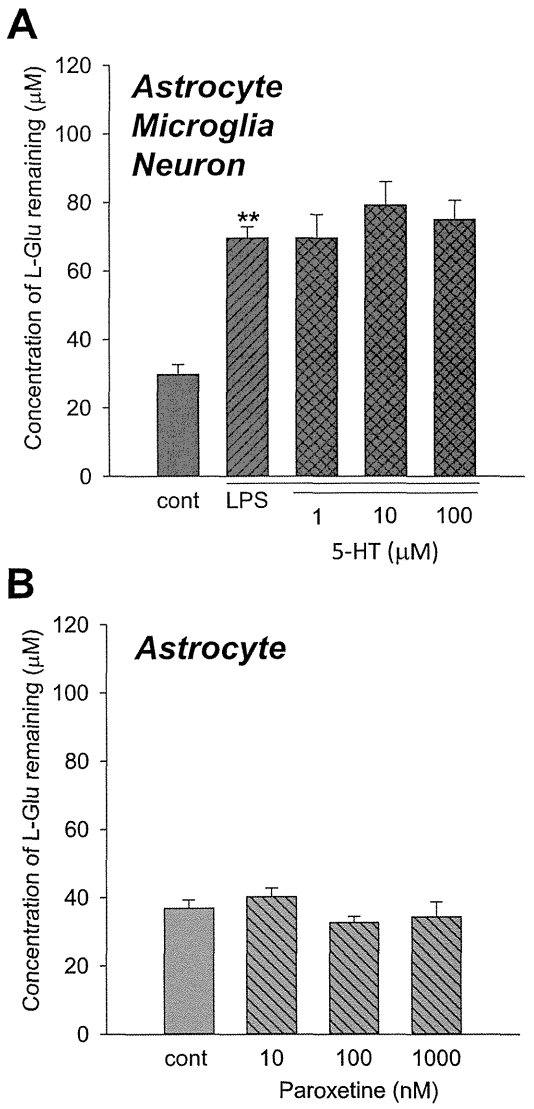

Fig. 2. Relation of the effects of paroxetine on LPS-induced decrease in L-Glu transport activity with its SSRI function and the direct effect on astrocytes. A. 72 h treatment with 5-HT (1–100 μM) did not affect LPS-induced decrease in the L-Glu transport activity. B. 72 h treatment with paroxetine (10–1000 nM) of astrocyte culture did not affect its L-Glu transport activity. **: $p < 0.01$ vs. control group, Tukey's test following ANOVA ($N = 6$).

The shape of microglia in the mixed culture was dramatically changed to amoeboid type by LPS and this morphological change was remarkably suppressed by paroxetine (unpublished observation). This suggests that paroxetine does not only suppress L-Glu release from microglia alone but also microglial activation. To demonstrate this possibility, the effect of paroxetine on the microglial activation is needed to be confirmed using multiple parameters. Because SSRIs have diverse chemical structures despite a common mode of action of 5-HT function (11), it is possible that paroxetine revealed the effects through interaction with paroxetine-specific target molecules. Because paroxetine exhibited the powerful inhibition of calcium influx via $P2X_4$ receptors (12), $P2X_4$ receptor is one of the most probable candidate molecules. The expression level of $P2X_4$ receptor in microglia is up-regulated in inflammatory pain model in spinal cord and is thought to be important for microglial inflammatory responses (13). MAPK signaling molecules (14) and GABA(B) receptor (15) are possibly involved in the paroxetine-specific effects as well. The effective concentration of paroxetine to reduce L-Glu release was 1 μM. According to the attached documents of paroxetine (http://www.info.pmda.go.jp/), intracerebral concentration of paroxetine reaches 77 nM by 25 mg/day-repeated administration. It is therefore unlikely that paroxetine affects astrocyte L-Glu transporters and microglia by the general dosage of SSRI. For clinical application of our present findings, further investigation concerning application period and dosage is needed.

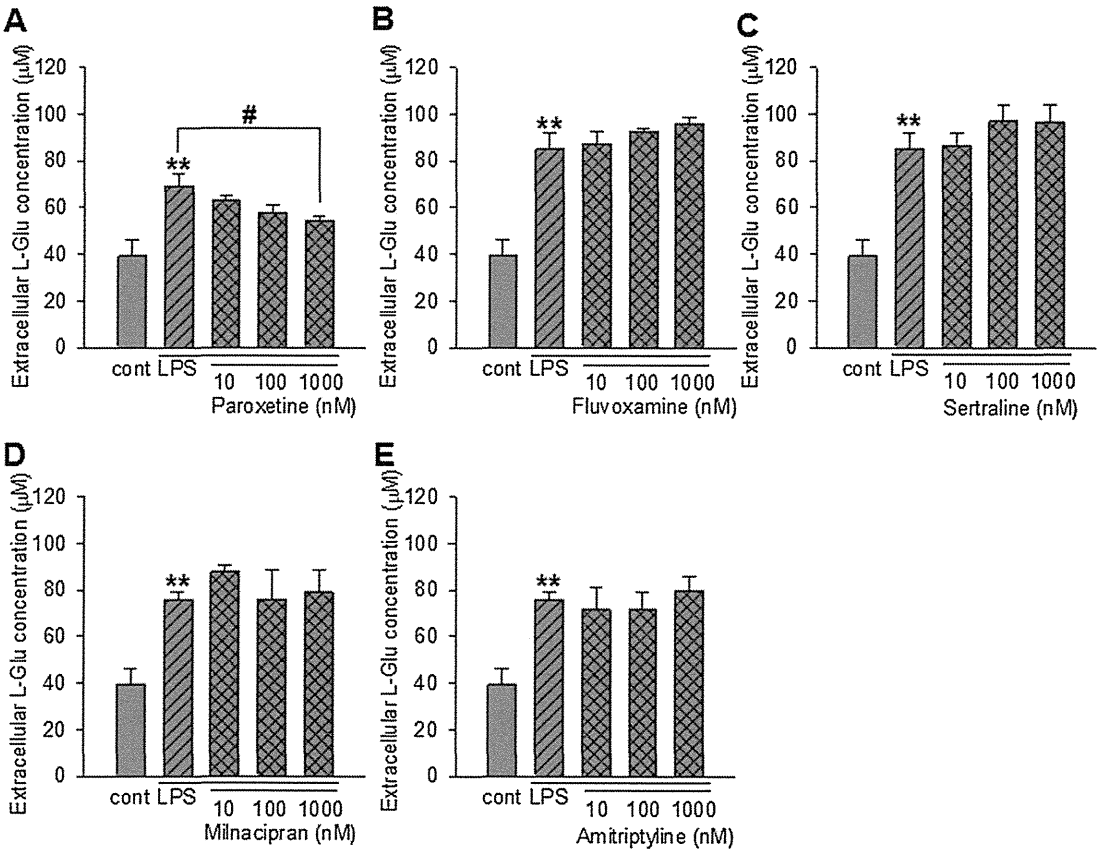

Fig. 3. Effects of antidepressants on the L-Glu release from microglia under the inflammatory condition. In each set of experiment, antidepressants were applied to the mixed culture from 1 h before to the end of the LPS-treatment (10 ng/ml, 24 h). The extracellular concentration of L-Glu was quantified. Paroxetine prevented the LPS-induced L-Glu release from microglia in a concentration-dependent manner (A). Fluvoxamine (B), sertraline (C), milnacipran (D), and amitriptyline (E) had no effects on LPS-induced L-Glu release from microglia. **: $p < 0.01$ vs. control group, #: $p < 0.05$ vs. LPS-treated group, Tukey's test following ANOVA ($N = 6$).

In conclusion, we found that paroxetine inhibit the L-Glu release from activated microglia and prevent down-regulation of astrocytic L-Glu transporters in the early stage of neuroinflammation. This is the novel pharmacological effect of paroxetine, which may bring advantages on the therapy of the disease associated with neuroinflammation.

Conflicts of interest

I declare that I have no significant competing financial, professional or personal interests that might have influenced the results and interpretation of the manuscript.

Author's contributions

K.F. performed experiments and manuscript writing.
J.T. performed experiments.
Y.S-M. provided advice on manuscript writing
Y.S. provided advice on manuscript writing
T.S. provided advice on the experimental direction and manuscript writing.
K.S. designed the experimental plan and performed experiments, manuscript writing.

Acknowledgments

This work was partly supported by a Grant-in-Aid for Young Scientists from Ministry of Education, Culture, Sports, Science, and Technology, Japan (KAKENHI 21700422), the Program for Promotion of Fundamental Studies in Health Sciences of National Institute of Biomedical Innovaton (10-21), Japan, a Health and Labor Science Research Grant for Research on Risks of Chemicals, a Labor Science Research Grant for Research on New Drug Development from the MHLW, Japan, awarded to K.S., Grant-in-Aid for research from MEXT, Japan (KAKENHI C23590113) awarded to T.S., and a Health and Labor Science Research Grant for Research on Publicly Essential Drugs and Medical Devices, Japan, awarded to Y.S.

References

(1) Bowerman M, Vincent T, Scamps F, Perrin FE, Camu W, Raoul C. Neuroimmunity dynamics and the development of therapeutic strategies for amyotrophic lateral sclerosis. Front Cell Neurosci. 2013;7:214.
(2) Liimatainen S, Lehtimaki K, Palmio J, Alapirtti T, Peltola J. Immunological perspectives of temporal lobe seizures. J Neuroimmunol. 2013;263:1–7.
(3) Schwartz M, Baruch K. The resolution of neuroinflammation in neurodegeneration: leukocyte recruitment via the choroid plexus. EMBO J. 2014;33:7–22.
(4) Lucas SM, Rothwell NJ, Gibson RM. The role of inflammation in CNS injury and disease. Br J Pharmacol. 2006;147(Suppl. 1):S232–S240.
(5) Masliah E, Alford M, DeTeresa R, Mallory M, Hansen L. Deficient glutamate transport is associated with neurodegeneration in Alzheimer's disease. Ann Neurol. 1996;40:759–766.
(6) Ferrarese C, Zoia C, Pecora N, Piolti R, Frigo M, Bianchi G, et al. Reduced platelet glutamate uptake in Parkinson's disease. J Neural Transm. 1999;106:685–692.
(7) Rothstein JD, Martin LJ, Kuncl RW. Decreased glutamate transport by the brain and spinal cord in amyotrophic lateral sclerosis. N Engl J Med. 1992;326:1464–1468.
(8) Takaki J, Fujimori K, Miura M, Suzuki T, Sekino Y, Sato K. L-glutamate released from activated microglia downregulates astrocytic L-glutamate transporter

expression in neuroinflammation: the 'collusion' hypothesis for increased extracellular L-glutamate concentration in neuroinflammation. J Neuroinflammation. 2012;9:275.
(9) Hashioka S, Klegeris A, Monji A, Kato T, Sawada M, McGeer PL, et al. Antidepressants inhibit interferon-gamma-induced microglial production of IL-6 and nitric oxide. Exp Neurol. 2007;206:33–42.
(10) Hwang J, Zheng LT, Ock J, Lee MG, Kim SH, Lee HW, et al. Inhibition of glial inflammatory activation and neurotoxicity by tricyclic antidepressants. Neuropharmacology. 2008;55:826–834.
(11) RJ B. Drugs and the treatment of psychiatrc disorders. Goodman and Gilman's the pharmacological basis of therapeutics. In: Hardman JG, Limbird LE, Gilman AG, editors. 10th ed 2001. p. 447–483.
(12) Nagata K, Imai T, Yamashita T, Tsuda M, Tozaki-Saitoh H, Inoue K. Antidepressants inhibit P2X4 receptor function: a possible involvement in neuropathic pain relief. Mol Pain. 2009;5:20.
(13) Guo LH, Trautmann K, Schluesener HJ. Expression of P2X4 receptor by lesional activated microglia during formalin-induced inflammatory pain. J Neuroimmunol. 2005;163:120–127.
(14) Liu RP, Zou M, Wang JY, Zhu JJ, Lai JM, Zhou LL, et al. Paroxetine ameliorates lipopolysaccharide-induced microglia activation via differential regulation of MAPK signaling. J Neuroinflammation. 2014;11:47.
(15) Khundakar AA, Zetterstrom TS. Effects of GABAB ligands alone and in combination with paroxetine on hippocampal BDNF gene expression. Eur J Pharmacol. 2011;671:33–38.

Fundamental Toxicological Sciences (Fund. Toxicol. Sci.)
Vol.1, No.3, 87-94, 2014

Original Article

Residual metals in carbon nanotubes suppress the proliferation of neural stem cells

Yukari Shigemoto-Mogami[1], Koki Fujimori[1,2], Yoshiaki Ikarashi[3], Akihiko Hirose[4], Yuko Sekino[1] and Kaoru Sato[1]

[1]Laboratory of Neuropharmacology, Division of Pharmacology, National Institute of Health Sciences, 1-18-1 Kamiyoga, Setagaya-ku, Tokyo 158-8501, Japan
[2]Division of Basic Biological Science, Faculty of Pharmacy, Keio University, 1-5-30 Shiba-koen, Minato-ku, Tokyo 105-8512, Japan
[3]Division of Environmental Chemistry, National Institute of Health Sciences, 1-18-1 Kamiyoga, Setagaya-ku, Tokyo 158-8501, Japan
[4]Division of Risk Assessment, National Institute of Health Sciences, 1-18-1 Kamiyoga, Setagaya-ku, Tokyo 158-8501, Japan

(Received October 17, 2014; Accepted October 20, 2014)

ABSTRACT — Carbon nanotubes (CNTs) are used in many fields; however, little is known about the effects of CNTs on the central nervous system (CNS). In this study, we found that extracts of sonicated CNTs suppressed the proliferation of neural stem cells (NSCs). Single-walled CNTs (SWCNTs) and multiple-walled CNTs (MWCNTs) were suspended in PBS (1 mg/mL) and sonicated for 5 hr using a water bath sonicator. Supernatants from both types of CNTs suppressed NSC proliferation. The effects weakened in a dilution-ratio-dependent manner and strengthened in a sonication time-dependent manner. Metal concentrations extracted from SCNTs and MCNTs after 5-hr of sonication were determined using inductively coupled plasma mass spectrometry. Mn, Rb, Cs, Tl, and Fe were detected in the SWCNT supernatant, and Mn, Cs, W, and Tl were detected in the MWCNT supernatant. The concentration of Mn, Rb, and Fe eluted from the SWCNTs and Rb eluted from MWCNTs following sonication were sufficient to suppress NSC proliferation alone. N-acetyl cysteine (NAC) and ascorbic acid (AA) reversed the effects of Mn and Fe and restored NSC proliferation. The effects of Rb and Tl were not affected by the antioxidants. Both antioxidants largely restored the suppression of NSC proliferation induced by the SWCNT and MWCNT supernatants. These results suggest that metals extracted from CNTs via a strong vibration energy can suppress NSC proliferation through ROS production by the extracted metals.

Key words: Carbon nanotube, Neural stem cell, Metals, Proliferation

INTRODUCTION

CNTs are fiber-shaped nanomaterials that consist of graphite hexagonal-mesh planes (graphene sheet) in a single-layer (single-walled carbon nanotubes (SWCNTs)) or in multiple layers with nest accumulation (multi-walled carbon nanotubes (MWCNTs)). The structure of SWCNTs is a honeycomb carbon lattice rolled into a cylinder, and the basic morphology consists of a sheet of tangled SWCNT (with a diameter of approximately 2 nm) bundles with diameters tens of nanometers in length. The structure of MWCNTs consists of honeycomb carbon lattices rolled into a multi-layer tubular shape, and the basic morphology is composed of particles of tangled MWCNTs with a diameter of approximately 30 nm. CNTs are used in many fields, including energy, healthcare, environment, materials, and electronics. However, adverse effects of CNTs on human health are poorly understood. Exposure to asbestos is known to cause asbestosis, bronchogenic carcinoma, mesothelioma, pleural fibrosis and pleural plaques, indicating that both the lungs and the pleura are targets of asbestos (Donaldson *et al.*, 2013). CNTs also exist as fibers or compact particles; thus, most studies concerning the adverse effects of CNTs have focused on lung toxicity (Jaurand *et al.*, 2009; Pacurari *et al.*, 2010) based on the fiber pathogenicity paradigm developed in the 1970-80s.

Correspondence: Kaoru Sato (E-mail: kasato@nihs.go.jp)

However, recent reports showed that nano-particles can cross the blood–brain barrier (BBB) and enter the brain (Sharma and Sharma, 2007). Furthermore, it has been suggested that the olfactory nerve pathway is a portal of entry into the CNS (Henriksson and Tjalve, 2000; Persson *et al.*, 2003; Mistry *et al.*, 2009; Balasubramanian *et al.*, 2013). Recent reports showed that MWCNTs are toxic to neural cells (Belyanskaya *et al.*, 2009; Xu *et al.*, 2009; Gavello *et al.*, 2012). Here, we investigated the effects of CNTs on the self-renewal of neural stem cells (NSCs). The mammalian CNS comprises various cell types, including neurons, astrocytes, and oligodendrocytes, and these cells differentiate from NSCs at specific brain developmental stages. Sufficient proliferation of NSCs before differentiation is essential to supply the neurons and glia required for brain function (Caviness *et al.*, 1995; Kriegstein and Alvarez-Buylla, 2009). In addition, NSCs are maintained in the subventricular zone and the hippocampal subgranular zone in the adult brain. Adult neurogenesis from these NSCs plays a key role in higher-order brain functions, such as cognition, learning and memory (Couillard-Despres *et al.*, 2011; Eisch and Petrik, 2012; Rolando and Taylor, 2014). Thus, the effects of CNTs on the proliferation of NSCs need to be determined for both of brain development and brain function. Here, we report that sonicated extracts of CNTs suppressed the proliferation of NSCs. We also determined that these effects were mediated through ROS produced by residual metals in the CNTs.

MATERIALS AND METHODS

Materials

CNTs (SWCNT: purity > 95%; Lot No.: SW1859; MWCNT: purity: > 98%; Lot No.: 04-12/10#1-(4)) were supplied by Nikkiso Co., Ltd. (Shizuoka, Japan). Both test materials were not coated or modified. The detailed physiochemical properties of Nikkiso CNTs have been previously reported (Ema *et al.*, 2011; Matsumoto *et al.*, 2012). Epidermal growth factor (EGF), $MnCl_2$, RbCl, $TlCl_3$, $FeCl_2$, $FeCl_3$, and NAC were purchased from Sigma (St. Louis, Mo, USA). Fibroblast growth factor 2 (FGF2) was purchased from PeproTech (Rocky Hill, NJ, USA). AA was purchased from WAKO (Osaka, Japan). The BrdU cell proliferation assay kit was purchased from Merck (Darmstadt, Germany). B27 supplement, TrypLE Select, FBS, and DMEM were purchased from Life Technologies (Grand Island, NY, USA).

Preparation of supernatants of sonicated CNT solutions

SWCNTs and MWCNTs were suspended in PBS (1 mg/mL) and sonicated for 10 min or 5 hr using a water bath-sonicator (Hitachi-Kokusai Electric Inc., Tokyo, Japan) at a frequency of 36 kHz and a watt density of 65 W/264 cm^2. The supernatants of sonicated CNT suspensions were diluted with culture medium 10- to 1,000-fold.

Rat neural stem cell (NSC) culture

Rat NSCs were cultured as previously described (Reynolds *et al.*, 1992; Hamanoue *et al.*, 2009) with slight modifications. Briefly, the telencephalons were dissected from embryonic day 16 (E16) rats of either sex in ice-cold DMEM/F12. The tissue was then minced and dispersed into single cells by pipetting. Cells were then cultured in DMEM/F12 containing B27 supplement (1/200), 20 ng/mL fibroblast growth factor 2 (FGF2) and 20 ng/mL epidermal growth factor (EGF) for 7 days. The primary neurospheres were incubated with TrypLE Select for 15 min and dissociated by pipetting. Single cells were seeded in 96-well plates for the proliferation assay.

Measurement of metal concentrations

CNTs were suspended in PBS (1 mg/mL) and sonicated for 5 hr using a water bath sonicator. The metal concentrations in the CNT supernatants were quantified using an inductively coupled plasma mass spectrometer (ICP-MS) (Agilent 7500ce ICP-MS, Agilent Technologies, Santa Clara, CA, USA) fitted with a collision/reaction cell in helium mode. We first detected metals at concentrations exceeding the detection limits using a semi-quantitative analysis. Next, we determined the concentration of the detected metals (i.e., Mn, Fe, Rb, Cs, W, and Tl) using a full quantitative analysis with calibration curves.

Treatment of NSCs with the supernatants of sonicated CNT suspensions, metals, and antioxidants

NSCs were treated with the supernatants of sonicated CNT suspensions, $MnCl_2$ (1-100 ppb), RbCl (1-100 ppb), $TlCl_3$ (0.1-10 ppb), $FeCl_2$ (100-10,000 ppb) or $FeCl_3$ (100-10,000 ppb) with or without 10 μM N-acetyl cysteine (NAC) or 10 μM ascorbic acid (AA) for 24 hr.

NSC proliferation assay

We quantified NSC proliferation according the instructions from the BrdU cell proliferation assay kit (Calbiochem, Hayward, CA, USA). The primary neurospheres were dissociated into single cells and seeded in 96-well plates at a density of 2 x 10^4 cells/

well. BrdU was added to the medium during the treatment of NSCs. After incubation, the cells were fixed, and BrdU-immuno-labeling was performed. The fluorescence intensities were used as a marker of proliferation. The fluorescence was measured at an excitation wavelength of 320 nm and emission wavelength of 460 nm with a fluorescence microplate reader (Spectra Max Microplate reader, Molecular Devices, Sunnyvale, CA, USA).

Data analysis and statistics

All data are shown as the mean ± S.E.M. The statistical analysis was performed using Student's *t*-test or an ANOVA followed by a Tukey's test. Differences were considered to be significant at $p < 0.05$.

RESULTS

SWCNTs and MWCNTs were suspended in PBS (1 mg/mL) and sonicated for 5 hr using a water bath sonicator. The supernatants of the sonicated CNT suspensions were collected and diluted with culture medium 10- to 1,000-fold. We found that a 24-hr treatment with supernatants of SWCNT and MWCNT suppressed NSC proliferation in a dilution ratio-dependent manner (Fig. 1). The suppression of proliferation was stronger with the SWCNT supernatant when compared with the MWCNT supernatant. The effects of sonication time were also assessed. The suppressive effects of both supernatants disappeared when the sonication time was changed from 5 hr to 10 min (Fig. 2). These results suggest that the suppression of NSC proliferation is due to factors released from CNTs in a sonication time-dependent manner.

CNTs are manufactured using metallic catalysts (Ding *et al.*, 2008; Yazyev and Pasquarello, 2008; Banhart, 2009; Tyagi *et al.*, 2011). Thus, we speculated that residual metals extracted from CNTs during the 5-hr sonication may be responsible for the suppression of NSC proliferation. We therefore quantified the metal contents in the CNT supernatants. The metals in the SWCNT and MWCNT supernatants were first analyzed using ICP-MS in a semi-quantitative mode. Next, the concentrations of metals were determined using calibration curves (Table 1). We found that a 5-hr sonication induced the extraction of multiple metals from the CNTs. Mn, Rb, Cs, Tl, and Fe were detected in the SWCNT supernatant, whereas Mn, Cs, W, and Tl were detected in the MWCNT supernatant. Among these metals, the concentration of Fe in SWCNT supernatant was remarkably high (from N.D. to 7,110 ppb). The concentrations of these metals in PBS were largely negligible and did not change after a 5-hr sonication.

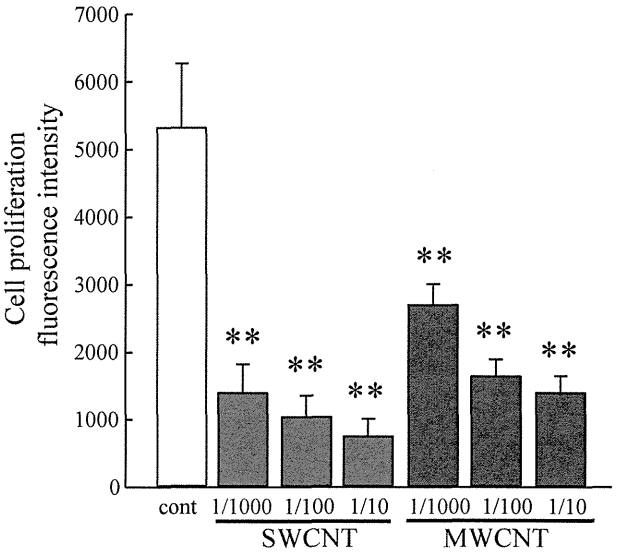

Fig. 1. Effects of the supernatants of sonicated CNT suspensions on the proliferation of rat NSCs. The supernatants of SWCNTs and MWCNTs suppressed NSC proliferation in a dilution ratio-dependent manner. *: $p < 0.05$, **: $p < 0.01$ vs. control group (N = 6), ANOVA followed by a Tukey's test.

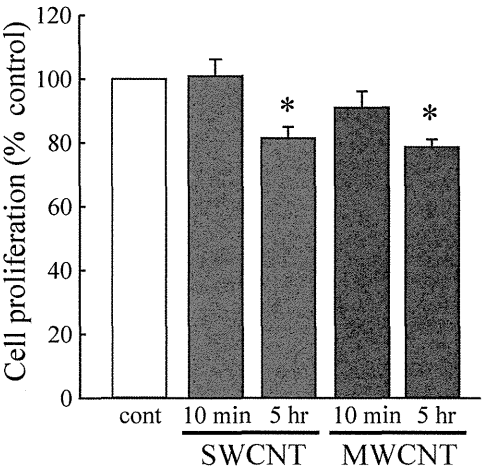

Fig. 2. Sonication time-dependence of CNT supernatant effects. The effects of SWCNT and MWCNT supernatants disappeared with a sonication time of 10 min. However, a 5-hr sonication time produced a significant suppression of NSC proliferation. *: $p < 0.05$ vs. control group (N = 6), ANOVA followed by a Tukey's test.

Next, we examined the direct effects of the metals at concentration ranges detected in the supernatants. Fig. 3 shows the metals that had a suppressive effect on NSC

Table 1. Metals eluted from CNTs by sonication for 5 hr.

	Concentrations of metals (ppb) 1 ppb = 10^{-8}%					
	PBS	PBS	SWCNT	SWCNT	MWCNT	MWCNT
sonication	-	+	-	+	-	+
Mn	nd	nd	0.33	16.04	nd	0.26
Rb	3.97	3.84	6.88	13.33	4.06	4.61
Cs	nd	nd	0.1	0.32	nd	0.59
W	nd	0.05	nd	0.08	nd	0.4
Tl	md	nd	0.05	0.17	nd	0.37
Fe	nd	nd	nd	7110	nd	nd

The metal concentrations in the supernatant of SWCNT and MWCNT were quantified using ICP-MS in a semi-quantitative mode followed by a full quantitative mode. Mn, Rb, Cs, W, Tl, and Fe were detected in the SWCNT supernatant. Mn, Rb, Cs, W, Tl, and Fe were detected in the MWCNT supernatant. The concentration of Fe in the SWCNT supernatant was remarkably high (7,110 ppb).

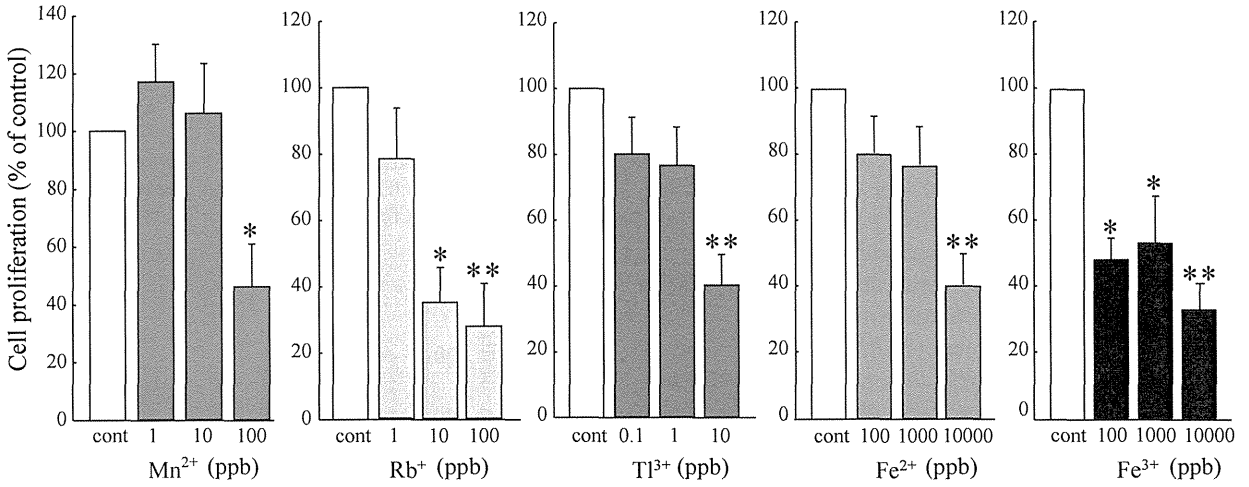

Fig. 3. The direct effect of metals in CNT supernatants. Mn^{2+}, Rb^{+}, Tl^{3+}, Fe^{2+}, and Fe^{3+} suppressed NSC proliferation in a concentration-dependent manner. *: $p < 0.05$, **: $p < 0.01$ vs. control group (N = 12), ANOVA followed by a Tukey's test.

proliferation (Fig. 3). Mn^{2+}, Rb^{+}, Tl^{3+}, Fe^{2+}, and Fe^{3+} suppressed the proliferation of NSCs in a concentration-dependent manner. These results indicate that Mn, Rb, and Fe were present in the SWCNT supernatant at a concentration high enough to suppress NSC proliferation. This effect was induced by the Rb in the MWCNT supernatant. Some metals are known to produce reactive oxygen species (Ding *et al.*, 2008) that can result in oxidative stress on lipids, DNA and proteins (Henriksson and Tjalve, 2000; Choi *et al.*, 2007; Alekseenko *et al.*, 2008; Kim *et al.*, 2011; Latronico *et al.*, 2013; Roth and Eichhorn, 2013; Sripetchwandee *et al.*, 2013). Thus, we examined the involvement of ROS in the suppression of NSC proliferation. N-acetyl cysteine (NAC) (10 μM) and ascorbic acid (AA) (10 μM) are typical antioxidants that can significantly restore the suppression of the NSC proliferation caused by Mn^{2+}, Fe^{2+}, and Fe^{3+} (Fig. 4A). The effect of Rb and Tl were not affected by NAC or AA (data not shown). These results suggest that ROS is involved in the suppressive effects produced by Mn and Fe. We also examined whether ROS played a role in the suppression of NSC proliferation by the CNT supernatants (Fig. 4B). Both NAC and AA markedly restored the decrease in NSC proliferation caused by the SWCNT and MWCNT supernatants. We confirmed that both of these antioxidants alone did not affect NSC proliferation (data not shown). Taken together, these results suggest that the suppressive effects of the sonicated extract of CNTs were mainly caused by

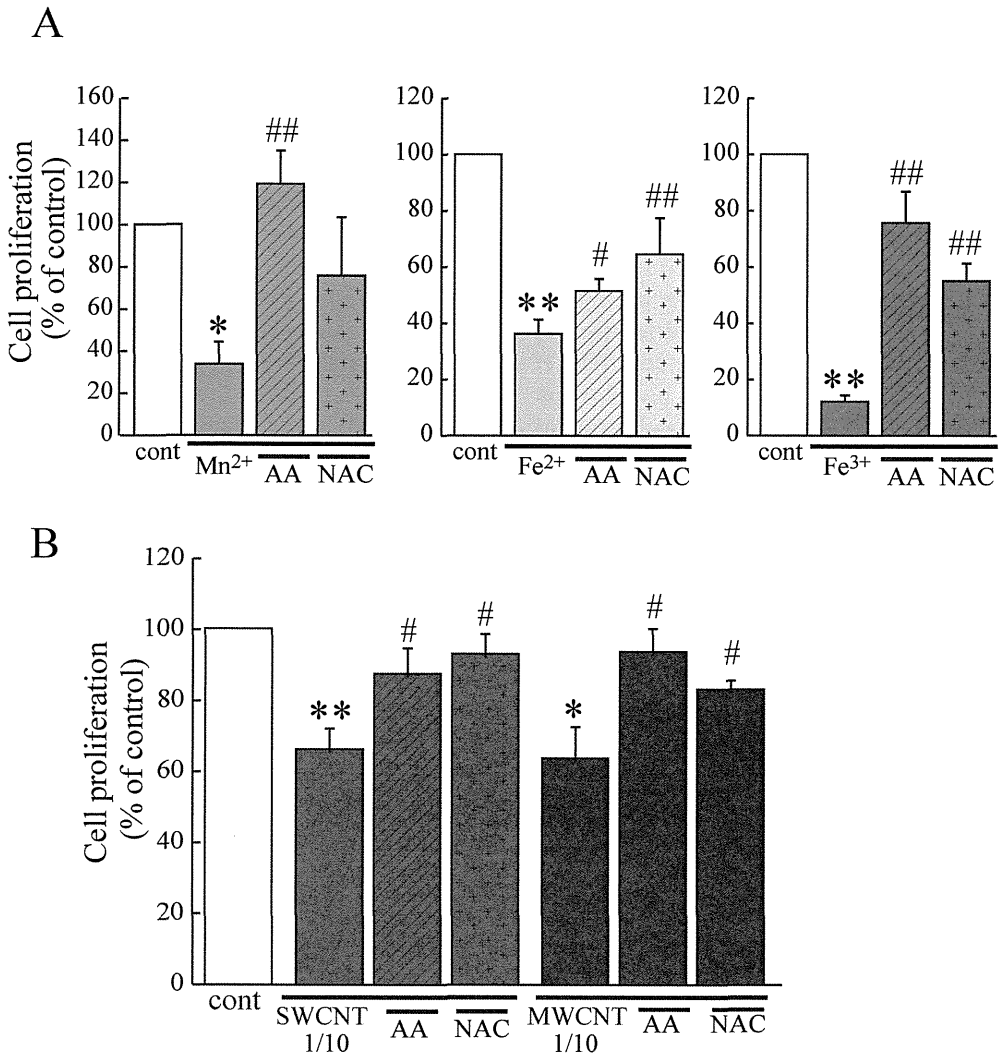

Fig. 4. Antioxidants attenuated the reduction in NSC proliferation caused by metals and CNT supernatants. The suppression of the NSC proliferation caused by Mn^{2+}, Fe^{2+}, Fe^{3+} (A) and the supernatants of CNTs (B) was significantly restored by NAC (10 μM) and AA (10 μM). *: $p < 0.05$,**: $p < 0.01$ vs. control group, #: $p < 0.05$, ##: $p < 0.01$ vs. metal or CNT-supernatant-treated groups (N = 7), ANOVA followed by a Tukey's test.

ROS produced by residual metals.

DISCUSSION

We found that the supernatants of sonicated CNT suspensions suppress NSC proliferation. We also determined that these effects were largely mediated by ROS production from residual metals. To demonstrate the involvement of ROS, we used the two antioxidants NAC and AA. NAC exerts its protective by increasing glutathione levels (Yim *et al.*, 1994; Arfsten *et al.*, 2007; Li *et al.*, 2009), directly scavenging ROS, and activating ERK1/2 (Zhang *et al.*, 2011). AA is a powerful water-soluble antioxidant that acts by scavenging ROS and reactive nitrogen species (Carr and Frei, 1999; Kojo, 2004). The concentrations of NAC and AA used in this study were at a level shown to suppress the effects of ROS in previous studies (Carr and Frei, 1999; De la Fuente and Victor, 2001; Nakajima *et al.*, 2009).

Proliferative NSCs have a high endogenous ROS lev-